Open Journal of Geology, 2025, 15(4), 199-219
https://www.scirp.org/journal/ojg
ISSN Online: 2161-7589
ISSN Print: 2161-7570

Preliminary Note on the Control of Gold Mineralization in South-West of Burkina Faso (West Africa): The Case of Zone B of the Gnimi-Yabogane Deposit

Saga Sawadogo[1,2*], Abraham Seydoux Traoré[1], Ousséný Sourgou[3], Rayangniwendé Abdoul Rasaky Kaboré[2]

[1]Geosciences and Environment Laboratory, Department of Earth Sciences, Joseph KI-ZERBO University, Ouagadougou, Burkina Faso
[2]Cooperative Society with Board of Directors Burkina Mining, Ouagadougou, Burkina Faso
[3]University Center of Manga, Norbert ZONGO University, Koudougou, Burkina Faso
Email: *sawadsaga@gmail.com

How to cite this paper: Sawadogo, S., Traoré, A.S., Sourgou, O. and Kaboré, R.A.R. (2025) Preliminary Note on the Control of Gold Mineralization in South-West of Burkina Faso (West Africa): The Case of Zone B of the Gnimi-Yabogane Deposit. *Open Journal of Geology*, **15**, 199-219.
https://doi.org/10.4236/ojg.2025.154009

Received: March 7, 2025
Accepted: March 30, 2025
Published: April 2, 2025

Abstract

Analysis of gold mineralization in the Gnimi-Yabogane B zone, in the commune of Dano in southwest Burkina Faso, within the Boromo greenstone belt, reveals local geology comprising volcano-sedimentary rocks, meta-andesite, amphibolitic gabbros, and granodiorites. The study highlighted three phases of deformation (D1, D2, D3), with mineralization mainly controlled by the D2 phase, responsible for the development of NE-SW shear corridors. Deformation markers show that the D1 shear zones are sinistral and the D2 dextral, with gold mainly associated with sulfide-rich brecciated smoky quartz veins. These results confirm structural control of the Mineralization at Area B of the Gnimi-Yabogane deposit in the southwest region.

Keywords

Mineralization, Deformation, Structures, Gnimi, Yaboghane

1. Introduction

The connection between the Congo Craton and the West African Craton is thought to have played a fundamental role in the geological processes that led to the formation of juvenile crust of Palaeoproterozoic age [1]-[7]. In the South Shield (Man/Leo) of the West African Craton, the geological formations are essentially of Palaeoproterozoic age, dominated by metavolcano-sedimentary belts and plutonic formations metamorphosed during the Eburnian orogeny (**Figure 1**). These processes began at the end of the Archean and concluded in the Palaeoproterozoic with the gradual installation of various types of granitoids [8] within the pre-existing volcanic and volcano-sedimentary formations.

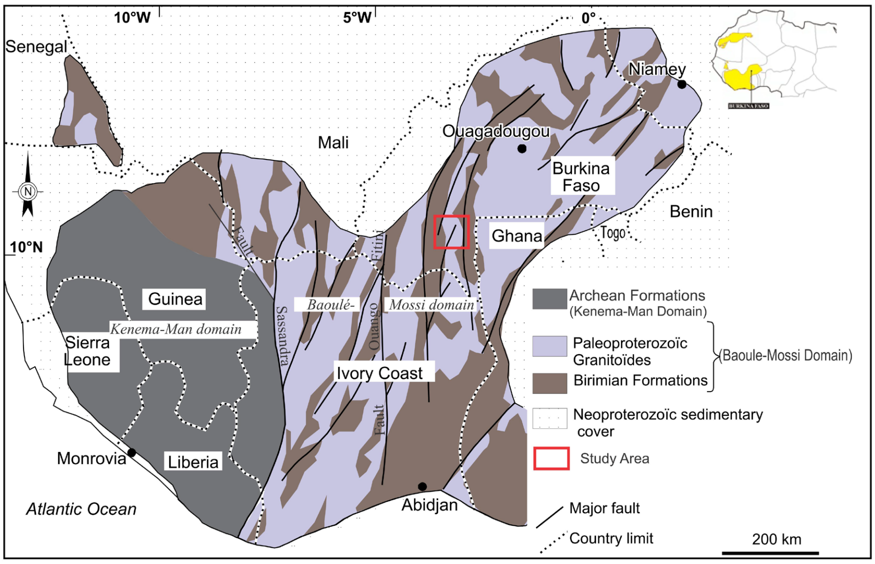

Figure 1. Simplified geological map of the Man/Leo Shield [20].

The Eburnian orogeny, coinciding with the emplacement of the granitoids, was marked by intense deformation and metamorphism affecting these formations. These tectonic and magmatic dynamics locally amplified the deformation and metamorphism, playing a key role in the structural and geological evolution of the region. The initial phase of deformation was characterised by regional shortening in an E-W direction, resulting from convergence between the Archean Kénéma-Man block and the Archean Congo craton block [9] [10]. This shortening, accompanied by the emplacement of granitoids, profoundly affected the volcanic and sedimentary rocks, leading to their metamorphism and deformation. The greenstone belt structure is the result of the combined effect of several geodynamic processes [11]-[13].

This initial deformation (D1) was then accommodated by more localised transcurrent tectonics, responsible for the D2 and D3 deformation phases [9]-[12]. The lithostratigraphy of the Birimian formations has long been the subject of scientific debate, but it has been established that these formations are underlain by a base of ultrabasic rocks that evolved into tholeiitic basalts, before ending in sediments intercalated with calc-alkaline volcanic rocks [12] [14] [15].

In parallel with this geological evolution, transcurrent tectonics generated major shear zones, notably the Tiébélé-Dori-Markoye fault in Burkina Faso, the Senegal-Malian fault, and the Sassandra fault in Côte d'Ivoire. These major structures were subsequently reactivated, favoring the development of secondary shear corridors, which are natural traps for economically exploitable mineralization. In most cases, this Mineralization is mainly controlled by tectonic structures, in addition to lithological factors [16]-[18]. The study area has been the subject of little scientific research since the 1960s [15] [19]. It is therefore essential to examine its gold potential and the factors that have controlled its mineralisation.

The aim of this study is to use field and laboratory data to analyze the factors controlling gold mineralization in Zone B of the Gnimi-Yabogane sector in southwest Burkina Faso. The research also aims to establish guiding criteria for drilling and gold prospecting in the region.

2. Regional Geological Context

From the 1960s to the present, the study area has been the subject of mapping and mining surveys [19] [21]-[23]. Petrographically, it is characterised by greenstone belts comprising mainly metavolcanic rocks (metabasalts, metaandesites, etc.), along with lesser amounts of metaplutonic rocks (metagabbros, metadiorites, etc.) and metasedimentary rocks (schists, metapelites, etc.). These formations are intersected by two distinct generations of granitoids. The first generation corresponds to the TTG granitoids (Tonalites, Trondhjemites, and Granodiorites), with a geochemical signature similar to Archean TTGs [2] [12] [17] [24] [25] or Andean adakites [26]. These granitoids structured the greenstone belts, giving them a N-S to NNE-SSW orientation and also induced contact metamorphism in the surrounding formations [27] [28]. A second generation of isotropic, biotite-only granitoids cuts through these formations.

In terms of metamorphism, the Boromo belt formations have been affected by greenschist to amphibolite facies metamorphism, with local hydrothermal manifestations. This metamorphism is accompanied by regional schistosity (S1), resulting from NW-SE trending shortening attributed to the first deformation phase (D1) of the Eburnian orogeny [15].

Structurally, three major shear zones cross the region. To the east, the Ouessa-Fara shear zone is a significant structure. In the center, the Dissine-Gnimi shear zone, also known as the Lopal anomaly, cuts directly through the study area (see **Figure 2**). To the west, the Bontioli-Bonzan shear zone completes the fault network. These shear corridors have facilitated the concentration of gold mineralization, as evidenced by the Gnimi and Yaboghane gold panning sites. These sites, located about 25 km from the commune of Dano and 330 km from Ouagadougou, illustrate the structuring role of these faults in controlling gold mineralization.

3. Methodology

The methodology for this study is based on four main areas: literature review, fieldwork, laboratory analysis, and data interpretation.

The literature review provided an overview of previous and current research in the study area.

Fieldwork involved systematic sampling at each outcrop site encountered and of the different facies traversed during core drilling. Petrographic and structural studies were conducted at these outcrop sites, while only petrographic studies were performed at the core drilling sites.

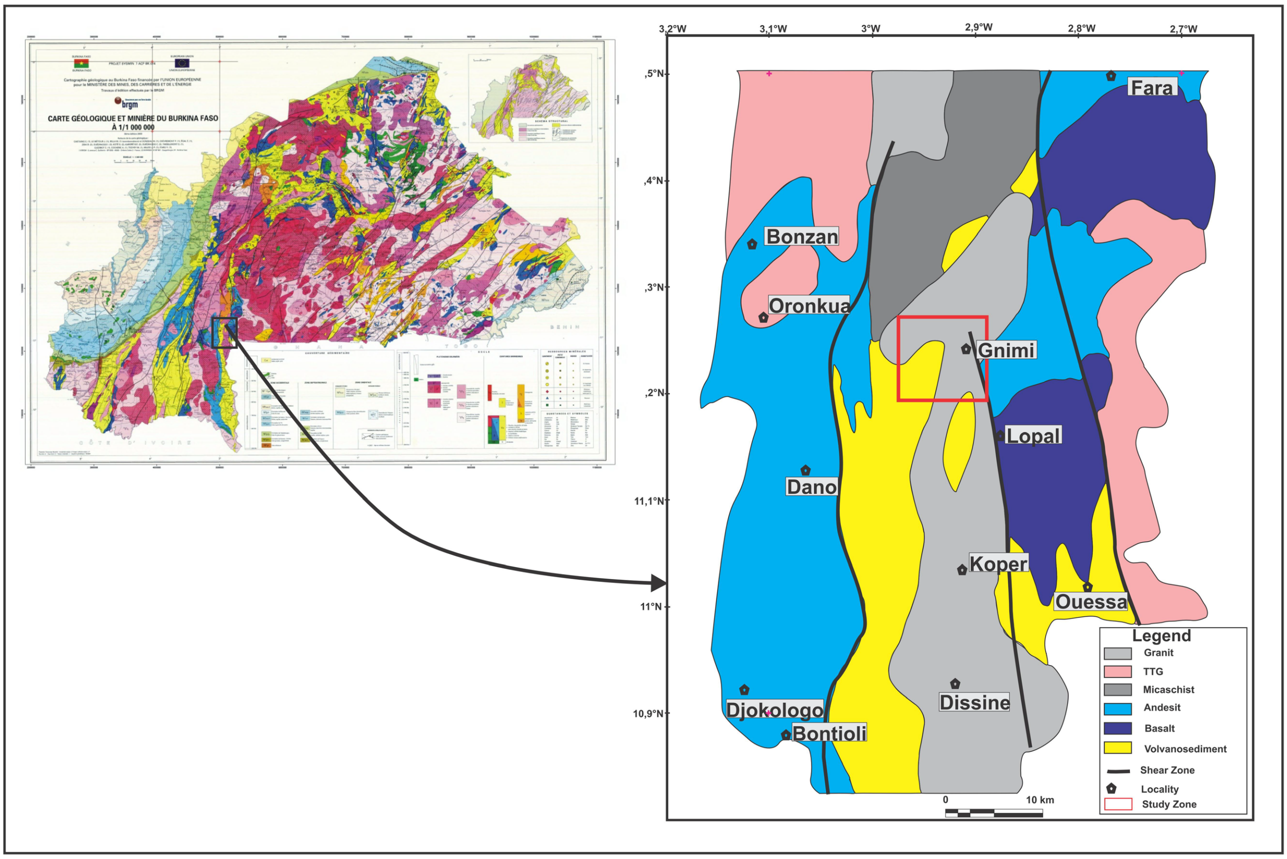

Figure 2. Geological map of the study area (extract from the geological map at 1/1,000,000 of Burkina Faso) [15].

Laboratory analyses included preparing thin sections for detailed petrographic and structural descriptions. Samples were also sent to ACLABS Burkina Faso SARL in Ouagadougou, Burkina Faso, for gold analysis to identify mineralized intercepts. These analyses of the mineralization control features were based on seven core holes with approximately 560 samples. Gold assaying was performed using the Au-Fire Assay AA (QOP AA-Au) method. Details of this assay method are available on the ACLABS laboratory website at http://www.actlabs.com. Finally, interpreting data from these stages helped refine the understanding of the lithological and structural controls on gold mineralization by establishing correlations between field observations and analytical results.

4. Results

4.1. Petrographic Characteristics

Macroscopic and microscopic observations identified three main rock types in the study area: metavolcano-sedimentary rocks, basic rocks (gabbros and metaandesites), and granitoids similar to the TTGs of the Dissine-Gnimi alignment, corresponding to the Lopal anomaly. The volcano-sedimentary rocks are exposed in certain localities such as Bontioli, Gnimi, Kayao, and Fara (**Figure 3a**). They mostly appear as highly weathered shales and are oriented according to the regional S1 schistosity, which trends N-S to NNE-SSW.

Microscopic analysis reveals that these rocks consist mainly of quartz and plagioclase phenocrysts. The presence of pressure shadows indicates zones of recrystallisation, testifying to the effects of metamorphism and deformation undergone by these formations (**Figure 3b**).

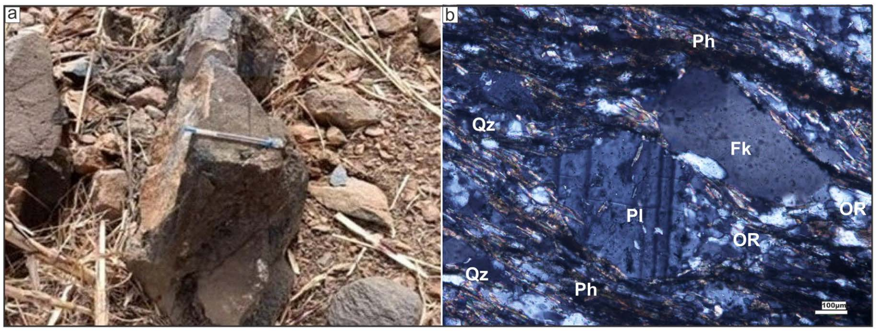

Figure 3. Volcano-sedimentary schists. a. Macroscopic image of schist outcrop. b. Microphotograph of volcano-sedimentary schists with plagioclase and potassium feldspar phenocrysts. Ph: Amphibole and biotite phyllites, Pl: Plagioclase, Fk: Potassium feldspar, Qz: Quartz, OR: Pressure shadow.

The basic facies intercalate with the volcanic-sedimentary schists that form their immediate host rock. They rarely surface but are present in gold panning rejects and core samples. These are gabbros with amphibolitic tendencies (**Figure 4a** and **Figure 4b**). Minerals such as amphibole, pyroxene, and plagioclase can be seen under the microscope. There are also dark-colored meta-andesites, sometimes grey, with a clear contact with the volcanic-sedimentary schists (**Figure 5a** and **Figure 5c**). Finally, there are dark-colored gabbros (**Figure 5b**), which microscopically consist mainly of amphibole, pyroxene, and plagioclase (**Figure 5d**).

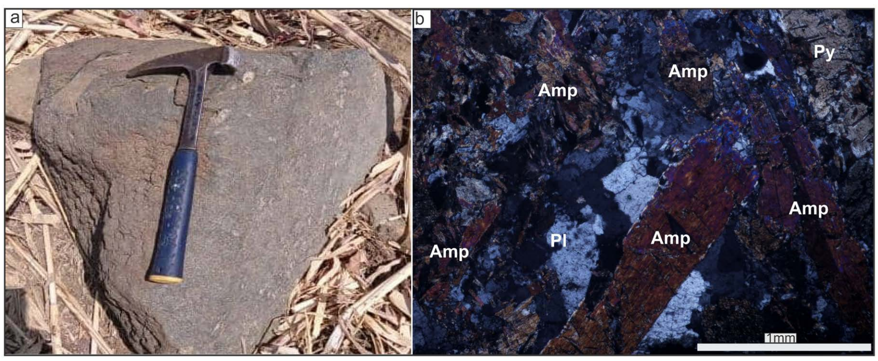

Figure 4. Amphibolitic gabbro. a. Outcrop. b. Microphotograph of an amphibolitic gabbro. Py: Pyroxene. Amp: Amphibole. Pl: Plagioclase.

Granitoids occur rarely and inconspicuously west of the mineralized zone. Two types of enclaves were identified: rounded enclaves, interpreted as comagmatic, and angular enclaves characterised by strong overmicassification (**Figure 6a**). Macroscopic observation reveals a high abundance of plagioclase, suggesting a granodioritic composition. These granitoids are intercalated in the greenstone belts they cross. Field relationships indicate they were emplaced within volcano-sedimentary formations. Microscopic analysis reveals minerals such as amphibole, biotite, plagioclase, and potassium feldspar, accompanied by accessory minerals like zircon, myrmekite, sphene, and epidote (**Figure 6b**).

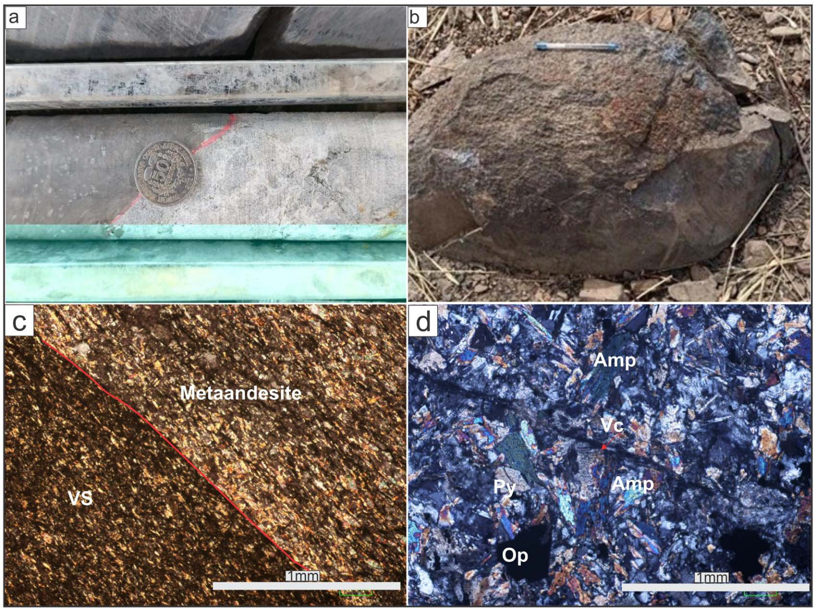

Figure 5. Macroscopic and microscopic illustrations of basic rocks. a. Macrophotograph of a core showing the contact between meta-andesite and volcano-sedimentary schist. b. Macrophotograph of a gabbro. c. Microphotograph of the contact between meta-andesite and volcano-sedimentary schist. d. Microphotograph of a gabbro. VS: Volcano-sedimentary, VC: Carbonate vein, Amp: Amphibole, Py: Pyroxene, Op: Opaque.

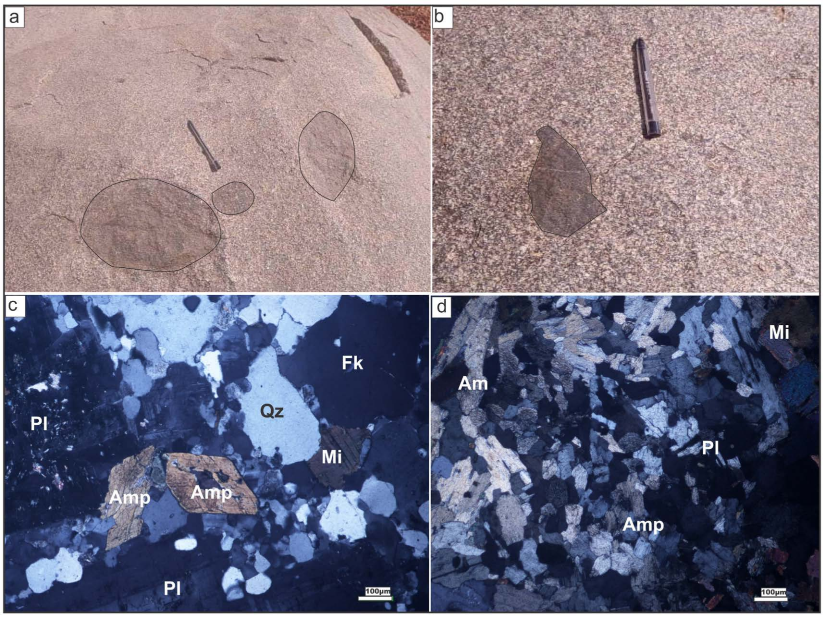

Figure 6. Illustrations of granodiorite and enclaves. a. Outcrop of granodiorite with co-magmatic enclaves. b. Outcrop of granodiorite with an angular overmicassed enclave. c. Microphotograph of a granodiorite. d. Microphotograph of an overmicassed enclave. AMP: Amphibole, Mi: Micas, Pl: Plagioclase, Fk: Potassium feldspar, Qz: Quartz.

4.2. Structural Analysis

In the field, the main structures observed locally include foliation, schistosity, folds, cracks, veins, and fractures. Schistosity comes in several variants. The N-S to NNE-SSW flow schistosity (S1) corresponds to the regional schistosity and highlights the alignment of the Boromo greenstone belt (**Figure 7a**). This D1 phase coincides with the emplacement of a wide range of first-generation TTG granitoids known in the eastern part of the Gnimi prospect. The structures are characterised by schistosity and first-order folding. Phase D1 is ductile and helped to straighten and shape the Birimian grooves of the Boromo greenstone belt. Phase D1 postdates gold mineralisation. It was overprinted by the D2 deformation phase, which develops in a deformation continuum of NNE-SSW to NE-SW-trending crenulation schistosity (S2) and second-order anisopic folds. This S2 played a key role in the continuity of the structuring of the volcano-sedimentary rocks and the TTG granitoids. D2 is semi-ductile and corresponds to sinistral shear zones. The structures of the D2 phase include foliation, crenulation schistosity, second-order folds, cracks, veins, and veins of smoky quartz and carbonate. The smoky quartz veins of this deformation phase are mined by gold miners.

The D3 deformation phase follows the D2 phase. In certain areas, depending on the competence of the formations, the foliation evolves towards mylonitic schistosity, indicating a high degree of deformation that creates S3 fracture schistosities.

Fracture schistosity (S3), associated with the latest tectonic events in the region, reflects the expression of phase D3 (**Figure 7b**). Furthermore, comagmatic enclaves and amphibolitic xenoliths present in the granitoids follow the orientation of the foliation, reinforcing its structural expression.

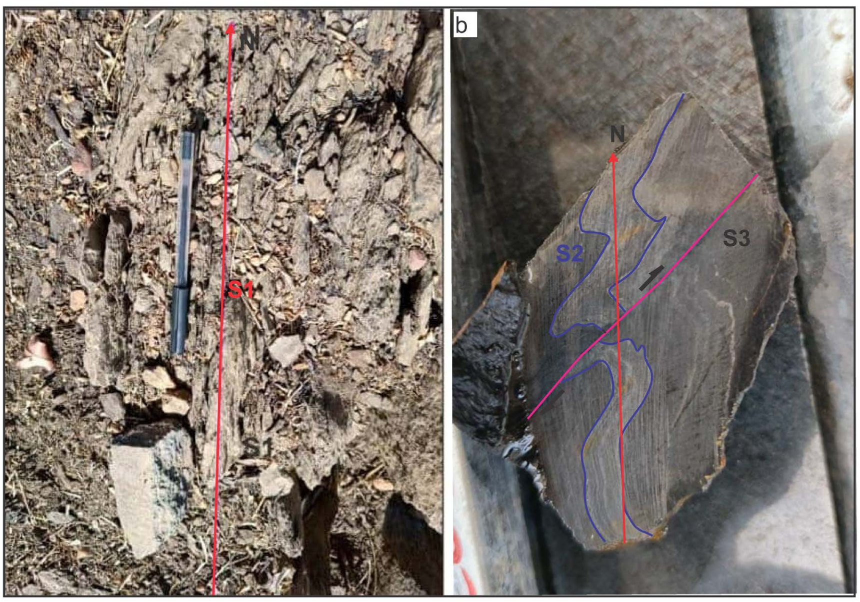

Figure 7. Illustrations of the different phases of deformation. a. Photographic illustration of the S1 schistosity with shear zones. b. Illustration of the S2 schistosity of the sinister D2 marked by first-order folding and S3 characterised by late fractures.

Comagmatic enclaves and xenoliths of amphibolitic composition also underline the foliation. The folds observed in the field are related to the crenulation schistosity (S2) and correspond to first-order folds (P1). Their development reflects the intensity of regional deformation in a deformation continuum.

The cracks of D2, mostly oriented NE-SW, are frequently filled with quartz, indicating fluid circulation associated with tectonic phases.

The veins fall into two main categories: quartz veins and carbonate veins (**Figure 8a**). Quartz veins have several orientations: some are aligned N-S, others NE-SW, while a final group follows an E-W direction. The carbonate veins are divided into two distinct generations: a first folded generation and a second unfolded generation, including a pleated first generation, which is D1, and a non-pleated second generation, which is D2.

The quartz veins observed in the study area fall into three distinct types, reflecting different phases of deformation. Smoky and brecciated quartz veins, the oldest, are associated with the D2 sinistral deformation phase and constitute the main mineralized structures. They are often accompanied by quartz veinlets, generally associated with sulfides, thus sharing a common history with smoky quartz. Finally, the white quartz veins, corresponding to the dextral D3 phase, are rarely mineralized and indicate more recent tectonic events (**Figure 8b**).

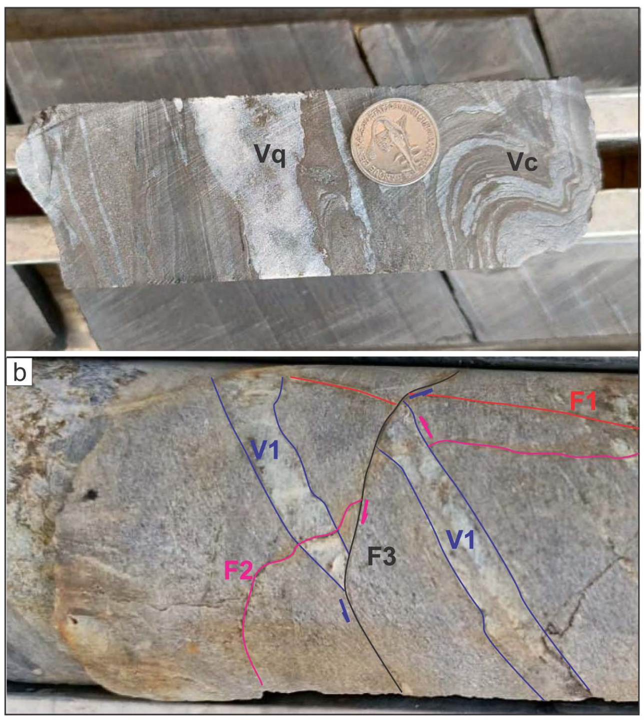

Figure 8. Quartz and carbonate veins and fractures; a. Illustrations of folded quartz veins (Vq) and carbonate veins (Vc). b. Quartz veins (V1) and three generations of fractures (F).

4.3. Mineralization Control

Laboratory assay results show gold grades ranging from 0.5 to 3 g/t, depending on the mineralized intercept (**Table 1**).

Table 1. Synthesis of mineralised intercepts.

Holes_ID	From	To	Au_ppm	Intercepts	Holes_ID	From	To	Au_ppm	Intercepts
GNM001B	1.7	2.7	0.025		GNM004B	41.6	42.75	0.019	
GNM001B	2.7	4	0.025		GNM004B	42.75	43.9	0.024	
GNM001B	4	5	0.019		GNM004B	43.9	45	0.021	
GNM001B	5	6	0.013		GNM004B	45	46.15	0.026	
GNM001B	6	7	0.009		GNM004B	46.15	47.2	0.015	
GNM001B	7	8	0.007		GNM004B	47.2	47.8	0.03	
GNM001B	8	10.6	0.005		GNM004B	47.8	49.5	0.012	
GNM001B	10.6	12.4	0.006		GNM004B	49.5	50.4	0.065	
GNM001B	12.4	14.1	<0.005		GNM004B	50.4	51.25	0.031	
GNM001B	14.1	15	<0.005		GNM004B	51.25	52.4	0.014	
GNM001B	15	16	0.008		GNM004B	52.4	53.5	0.042	
GNM001B	16	18	0.006		GNM004B	53.5	54.6	0.019	
GNM001B	18	20	0.009		GNM004B	54.6	55.7	0.012	
GNM001B	20	22.5	<0.005		GNM004B	55.7	56.8	0.015	
GNM001B	22.5	23.5	<0.005		GNM004B	56.8	57.9	0.028	
GNM001B	23.5	24.7	<0.005		GNM004B	57.9	59	0.021	
GNM001B	24.7	26.35	0.006		GNM005B	1.5	4.8	0.02	
GNM001B	26.35	30	<0.005		GNM005B	4.8	5.7	0.011	
GNM001B	30	31.5	0.005		GNM005B	5.7	7.1	0.015	
GNM001B	31.5	32.85	0.005		GNM005B	7.1	11.25	0.154	
GNM001B	32.85	33.9	0.006		GNM005B	11.25	14.36	0.028	
GNM001B	33.9	35.1	<0.005		GNM005B	14.36	17	0.112	
GNM001B	35.1	36.2	<0.005		GNM005B	17	18.5	0.16	
GNM001B	36.2	38	0.008		GNM005B	18.5	19.5	0.571	1m@0.571ppm
GNM001B	38	39.15	0.005		GNM005B	19.5	21.3	0.032	
GNM001B	39.15	40.2	0.006		GNM005B	21.3	23.2	0.407	1.9m@0.407ppm
GNM001B	40.2	40.7	0.005		GNM005B	23.2	24.1	0.272	
GNM001B	40.7	41.54	<0.005		GNM005B	24.1	26.15	0.058	
GNM001B	41.54	42.45	<0.005		GNM005B	26.15	27.7	0.089	
GNM001B	42.45	44.1	0.012		GNM005B	27.7	28.65	0.105	
GNM001B	44.1	45	0.005		GNM005B	28.65	29.6	0.023	
GNM001B	45	46.1	0.007		GNM005B	29.6	31	0.062	
GNM001B	46.1	47.26	0.006		GNM005B	31	32.32	3.77	2.45m@2.01ppm
GNM001B	47.26	48.55	0.015		GNM005B	32.32	33.45	0.257	
GNM001B	48.55	49.5	0.02		GNM005B	33.45	34.6	0.161	
GNM001B	49.5	50.5	0.03		GNM005B	34.6	35.75	0.215	

Continued

GNM001B	50.5	51.45	0.024	GNM005B	35.75	36.62	0.052	
GNM001B	51.45	52.6	0.188	GNM005B	36.62	37.45	4.02	
GNM001B	52.6	53.8	0.027	GNM005B	37.45	38.1	2.52	2.38m@2.29ppm
GNM001B	53.8	54.95	0.017	GNM005B	38.1	39	0.347	
GNM001B	54.95	56.2	0.037	GNM005B	39	39.8	0.064	
GNM001B	56.2	57.1	0.018	GNM005B	39.8	41	0.02	
GNM001B	57.1	58.2	0.025	GNM005B	41	42	0.018	
GNM001B	58.2	59.2	0.008	GNM005B	42	43	0.024	
GNM001B	59.2	60.4	0.008	GNM005B	43	43.9	0.011	
GNM001B	60.4	61.15	0.01	GNM005B	43.9	44.7	0.037	
GNM001B	61.15	62.3	0.023	GNM005B	44.7	46	0.024	
GNM001B	62.3	63.3	0.018	GNM005B	46	47	<0.005	
GNM001B	63.3	64.5	0.198	GNM005B	47	47.9	<0.005	
GNM001B	64.5	65.5	0.021	GNM005B	47.9	48.7	<0.005	
GNM001B	65.5	66.5	0.009	GNM005B	48.7	49.85	0.039	
GNM001B	66.5	67.5	0.009	GNM005B	49.85	50.9	0.006	
GNM001B	67.5	68.55	0.009	GNM005B	50.9	51.9	<0.005	
GNM001B	68.55	69.35	0.008	GNM005B	51.9	52.55	0.009	
GNM001B	69.35	70.5	0.043	GNM005B	52.55	53.5	<0.005	
GNM001B	70.5	71.65	0.006	GNM005B	53.5	54.5	0.006	
GNM001B	71.65	72.8	0.016	GNM005B	54.5	55.45	0.008	
GNM001B	72.8	73.95	0.008	GNM005B	55.45	56.4	0.009	
GNM001B	73.95	75.1	0.007	GNM005B	56.4	57.4	0.029	
GNM001B	75.1	75.95	0.006	GNM005B	57.4	58.45	0.254	
GNM001B	75.95	76.8	0.015	GNM005B	58.45	59.45	0.294	
GNM001B	76.8	77.7	0.075	GNM005B	59.45	60.75	0.077	
GNM001B	77.7	78.6	0.208	GNM005B	60.75	61.8	<0.005	
GNM001B	78.6	79.5	0.162	GNM005B	61.8	62.8	0.185	
GNM001B	79.5	80.65	0.013	GNM005B	62.8	63.9	0.281	
GNM001B	80.65	81.8	0.016	GNM005B	63.9	64.9	0.01	
GNM001B	81.8	83	0.175	GNM005B	64.9	65.7	0.237	
GNM001B	83	84.2	0.054	GNM005B	65.7	66.7	1.83	1.9m@1.15ppm
GNM001B	84.2	85.4	0.227	GNM005B	66.7	67.6	0.487	
GNM001B	85.4	86.8	0.014	GNM005B	67.6	68.25	0.017	
GNM001B	86.8	88.05	0.057	GNM005B	68.25	69.1	0.387	
GNM001B	88.05	89	0.008	GNM005B	69.1	70	0.03	
GNM001B	89	90	0.007	GNM005B	70	71	0.013	

Continued

GNM001B	90	91	0.007	GNM005B	71	71.9	0.01
GNM001B	91	92	0.012	GNM005B	71.9	72.8	0.017
GNM001B	92	93.4	0.022	GNM005B	72.8	73.75	0.012
GNM001B	93.4	94.5	0.074	GNM005B	73.75	74.85	0.013
GNM001B	94.5	95.6	0.007	GNM005B	74.85	76	0.01
GNM001B	95.6	96.9	0.008	GNM005B	76	77.15	0.016
GNM001B	96.95	98	0.01	GNM005B	77.15	78	0.026
GNM001B	98	99	0.008	GNM005B	78	79	0.026
GNM002B	0	1.55	0.031	GNM005B	79	80	0.077
GNM002B	1.55	3	0.007	GNM005B	80	80.85	<0.005
GNM002B	3	4.7	0.01	GNM005B	80.85	82	0.007
GNM002B	4.7	6	0.011	GNM005B	82	83	0.01
GNM002B	6	7.05	0.02	GNM005B	83	84.2	0.007
GNM002B	7.05	8.55	0.022	GNM005B	84.2	85.4	0.009
GNM002B	8.55	9.9	0.01	GNM005B	85.4	86.6	0.01
GNM002B	9.9	11	0.009	GNM005B	86.6	87.8	0.014
GNM002B	11	11.65	0.009	GNM005B	87.8	89	0.011
GNM002B	11.65	12.7	0.011	GNM005B	89	90	0.012
GNM002B	12.7	13.8	0.008	GNM005B	90	91.1	0.01
GNM002B	13.8	15	0.009	GNM005B	91.1	92.1	0.007
GNM002B	15	16.6	0.009	GNM005B	92.1	93	0.01
GNM002B	16.6	18	0.008	GNM005B	93	94	0.012
GNM002B	18	19.4	0.008	GNM005B	94	95.1	0.078
GNM002B	19.4	20.6	0.009	GNM005B	95.1	96.4	0.155
GNM002B	20.6	22.3	0.01	GNM005B	96.4	97.6	0.011
GNM002B	22.3	24	0.011	GNM005B	97.6	98.8	0.005
GNM002B	24	25.5	0.01	GNM005B	98.8	100	0.013
GNM002B	25.5	27	0.009	GNM006B	1.5O	4.5	0.018
GNM002B	27	28.5	0.009	GNM006B	4.5	6	0.008
GNM002B	28.5	29.8	0.009	GNM006B	6	7.7	0.012
GNM002B	29.8	31.1	0.011	GNM006B	7.7	10.5	0.012
GNM002B	31.1	33.3	0.009	GNM006B	10.5	12	0.02
GNM002B	33.3	34.3	0.011	GNM006B	12	13.5	0.009
GNM002B	34.3	35.3	0.044	GNM006B	13.5	14.2	0.005
GNM002B	35.3	36.4	0.015	GNM006B	14.2	14.85	0.01
GNM002B	36.4	37.5	0.014	GNM006B	14.85	16	0.013
GNM002B	37.5	38.6	0.017	GNM006B	16	17.15	0.01

Continued

GNM002B	38.6	39.7	1.27	2.25m@0.75ppm	GNM006B	17.15	19.5	0.105	
GNM002B	39.7	40.85	0.237		GNM006B	19.5	20.8	0.063	
GNM002B	40.85	42	0.024		GNM006B	20.8	22.2	0.154	
GNM002B	42	43	0.019		GNM006B	22.2	24	0.049	
GNM002B	43	44	0.093		GNM006B	24	26	0.053	
GNM002B	44	44.8	0.144		GNM006B	26	27.6	0.02	
GNM002B	44.8	45.45	0.024		GNM006B	27.6	28.65	0.013	
GNM002B	45.45	46.55	1.05		GNM006B	28.65	29.6	0.085	
GNM002B	46.55	47.8	0.478	4.45m@0.77ppm	GNM006B	29.6	31.5	0.026	
GNM002B	47.8	49	1.01		GNM006B	31.5	32.4	0.077	
GNM002B	49	49.9	0.554		GNM006B	32.4	33.25	0.011	
GNM002B	49.9	51	0.231		GNM006B	33.25	34.3	<0.005	
GNM002B	51	52	0.056		GNM006B	34.3	35.2	0.021	
GNM002B	52	53	0.184		GNM006B	35.2	36.2	0.024	
GNM002B	53	54	0.015		GNM006B	36.2	37.55	0.009	
GNM002B	54	54.9	0.02		GNM006B	37.55	39.5	0.082	
GNM002B	54.9	55.75	0.028		GNM006B	39.5	41	0.155	
GNM002B	55.75	56.6	0.057		GNM006B	41	42.8	0.023	
GNM002B	56.6	57.7	0.037		GNM006B	42.8	44	0.038	
GNM002B	57.7	58.7	0.051		GNM006B	44	44.9	0.135	
GNM002B	58.7	59.65	0.565		GNM006B	44.9	45.6	0.047	
GNM002B	59.65	61	0.043		GNM006B	45.6	46.55	0.408	
GNM002B	61	62.1	1.96		GNM006B	46.55	47.46	0.064	
GNM002B	62.1	63.25	1.38	3.7m@1.22ppm	GNM006B	47.46	48.2	0.235	
GNM002B	63.25	64.7	0.327		GNM006B	48.2	49.05	1.97	2.05m@1.53ppm
GNM002B	64.7	65.65	0.154		GNM006B	49.05	50.25	1.1	
GNM002B	65.65	66.8	0.017		GNM006B	50.25	51	0.009	
GNM002B	66.8	67.9	0.014		GNM006B	51	51.9	0.319	
GNM002B	67.9	69	0.018		GNM006B	51.9	53	0.053	
GNM002B	69	70.1	0.029		GNM006B	53	54	0.014	
GNM002B	70.1	71.3	0.331		GNM006B	54	55	0.021	
GNM002B	71.3	72.1	0.021		GNM006B	55	55.9	0.145	
GNM002B	72.1	73.1	0.031		GNM006B	55.9	56.9	0.017	
GNM002B	73.1	74	0.013		GNM006B	56.9	57.85	0.034	
GNM002B	74	75	0.02		GNM006B	57.85	58.95	0.051	
GNM002B	75	76.05	0.024		GNM006B	58.95	60	0.009	
GNM002B	76.05	76.85	0.023		GNM006B	60	60.95	0.016	

Continued

GNM002B	76.85	77.8	0.674		GNM006B	60.95	61.85	0.696	0.9m@0.696ppm
GNM002B	77.8	79	0.019		GNM006B	61.85	62.8	0.36	
GNM002B	79	80.2	0.016		GNM006B	62.8	63.55	0.261	
GNM002B	80.2	81.4	0.016		GNM006B	63.55	64.5	0.076	
GNM002B	81.4	82.6	0.017		GNM006B	64.5	65.5	0.006	
GNM002B	82.6	83.8	0.018		GNM006B	65.5	66.2	0.009	
GNM002B	83.8	85	0.014		GNM006B	66.2	66.9	0.005	
GNM002B	85	86.2	0.012		GNM006B	66.9	67.9	0.022	
GNM002B	86.2	87.4	0.015		GNM006B	67.9	68.8	0.03	
GNM002B	87.4	88.6	0.014		GNM006B	68.8	69.9	0.102	
GNM002B	88.6	89.8	0.012		GNM006B	69.9	71	1.57	6.25m@0.85ppm
GNM002B	89.8	91	0.011		GNM006B	71	72	1.05	
GNM002B	91	92	0.009		GNM006B	72	73	0.712	
GNM002B	92	93.05	0.013		GNM006B	73	74	0.047	
GNM002B	93.05	94.1	0.137		GNM006B	74	75	1.41	
GNM002B	94.1	95.15	0.26		GNM006B	75	76.15	0.291	
GNM002B	95.15	96.4	0.014		GNM006B	76.15	77	0.197	
GNM002B	96.4	97.6	<0.005		GNM006B	77	78	0.109	
GNM002B	97.6	98.8	<0.005		GNM006B	78	79	0.008	
GNM002B	98.8	100	<0.005		GNM006B	79	80.1	0.005	
GNM003B	0	1.5	0.026		GNM006B	80.1	81.43	0.005	
GNM003B	1.5	3.1	<0.005		GNM006B	81.43	82.3	0.049	
GNM003B	3.1	6	0.008		GNM006B	82.3	83.1	0.023	
GNM003B	6	7.5	0.005		GNM006B	83.1	84.05	0.022	
GNM003B	7.5	9.15	0.006		GNM006B	84.05	85.25	0.012	
GNM003B	9.15	10.05	0.006		GNM006B	85.25	86.3	0.014	
GNM003B	10.05	11	0.008		GNM006B	86.3	87.45	0.017	
GNM003B	11	12	0.009		GNM006B	87.45	88.6	0.014	
GNM003B	12	13.5	0.008		GNM006B	88.6	89.9	0.006	
GNM003B	13.5	15.55	0.433		GNM006B	89.9	91.05	0.218	
GNM003B	15.55	16.5	0.069		GNM006B	91.05	92	0.017	
GNM003B	16.5	17.05	0.046		GNM006B	92	93	0.013	
GNM003B	17.05	18.3	2.12	2.45m@1.17ppm	GNM006B	93	94	0.01	
GNM003B	18.3	19.5	0.227		GNM006B	94	95	0.012	
GNM003B	19.5	21.15	0.135		GNM006B	95	96	0.01	
GNM003B	21.15	22.55	0.167		GNM006B	96	97	0.01	
GNM003B	22.55	23.6	0.042		GNM006B	97	98	0.006	

Continued

GNM003B	23.6	24.7	0.008		GNM006B	98	98.8	0.005	
GNM003B	24.7	25.5	0.01		GNM006B	98.8	99.75	0.008	
GNM003B	25.5	26.3	0.019		GNM006B	99.75	100.65	0.036	
GNM003B	26.3	27.1	0.02		GNM006B	100.65	102	<0.005	
GNM003B	27.15	27.95	0.042		GNM006B	102	103.25	0.006	
GNM003B	27.95	29	0.04		GNM006B	103.25	104.15	<0.005	
GNM003B	29	30	1.14	1m@1.14ppm	GNM006B	104.15	105	0.04	
GNM003B	30	31.1	0.025		GNM007B	1.5	3	0.023	
GNM003B	31.15	32.1	0.236		GNM007B	3	3.85	0.012	
GNM003B	32.17	33.2	0.534	1.03m@0.534ppm	GNM007B	3.85	4.7	0.011	
GNM003B	33.2	34.2	0.086		GNM007B	4.7	5.8	0.018	
GNM003B	34.2	35.3	0.024		GNM007B	5.8	7	0.013	
GNM003B	35.3	36.2	0.012		GNM007B	7	8	0.008	
GNM003B	36.2	37.1	3.34	0.9m@3.34ppm	GNM007B	8	9	0.007	
GNM003B	37.1	38	0.014		GNM007B	9	10	0.016	
GNM003B	38	39	0.014		GNM007B	10	11	0.03	
GNM003B	39	40.0	0.012		GNM007B	11	12	0.012	
GNM003B	40.05	41.15	0.008		GNM007B	12	13	<0.005	
GNM003B	41.15	42	0.008		GNM007B	13	14	0.006	
GNM003B	42	42.9	0.663	0.95m@0.66ppm	GNM007B	14	14.9	<0.005	
GNM003B	42.95	44	0.031		GNM007B	14.9	15.65	0.012	
GNM003B	44	45.05	0.121		GNM007B	15.65	16.9	<0.005	
GNM003B	45.05	46.25	0.459	1.2m@0.459ppm	GNM007B	16.9	18	0.026	
GNM003B	46.25	47.35	0.185		GNM007B	18	19.5	<0.005	
GNM003B	47.35	48.73	0.035		GNM007B	19.5	20.25	<0.005	
GNM003B	48.73	50	0.024		GNM007B	20.25	21.93	<0.005	
GNM003B	50	51.35	0.077		GNM007B	21.93	23.05	0.008	
GNM003B	51.35	52.35	0.021		GNM007B	23.05	24.1	0.015	
GNM003B	52.35	53.4	0.021		GNM007B	24.1	25.5	0.338	3.85m@0.94ppm
GNM003B	53.4	54.4	0.014		GNM007B	25.5	27.95	1.55	
GNM003B	54.4	55.4	0.015		GNM007B	27.95	29.2	0.015	
GNM003B	55.4	56.45	0.037		GNM007B	29.2	31	0.022	
GNM003B	56.45	57.45	0.018		GNM007B	31	32	0.006	
GNM003B	57.45	58.35	0.01		GNM007B	32	33	0.014	
GNM003B	58.35	59.3	0.011		GNM007B	33	34	0.013	
GNM003B	59.3	60.25	0.282		GNM007B	34	35.15	0.008	
GNM003B	60.25	61.15	0.548	3.70m@0.63ppm	GNM007B	35.15	36	<0.005	

Continued

GNM003B	61.15	62	0.404	GNM007B	36	37.4	<0.005
GNM003B	62	63	1.22	GNM007B	37.4	38.6	<0.005
GNM003B	63	63.95	0.357	GNM007B	38.6	40.5	0.025
GNM003B	63.95	65.2	0.039	GNM007B	40.5	41.8	0.042
GNM003B	65.2	66.4	0.015	GNM007B	41.8	43	<0.005
GNM003B	66.4	67.6	0.022	GNM007B	43	44.3	<0.005
GNM003B	67.6	68.85	0.008	GNM007B	44.3	45.4	0.007
GNM003B	68.85	70.1	0.01	GNM007B	45.4	46.6	0.016
GNM003B	70.1	71.2	0.01	GNM007B	46.6	47.95	<0.005
GNM003B	71.2	72.3	0.012	GNM007B	47.95	49.1	0.105
GNM003B	72.3	73.3	0.009	GNM007B	49.1	50.25	0.01
GNM003B	73.3	74.35	0.009	GNM007B	50.25	51.36	0.007
GNM003B	74.35	75.4	0.029	GNM007B	51.36	52.46	0.005
GNM003B	75.4	76.4	0.067	GNM007B	52.46	53.63	0.007
GNM003B	76.4	77.5	0.022	GNM007B	53.63	54.74	0.005
GNM003B	77.5	78.7	0.053	GNM007B	54.74	55.84	0.019
GNM003B	78.7	79.9	0.143	GNM007B	55.84	56.94	0.007
GNM003B	79.9	81.15	0.127	GNM007B	56.94	58	0.035
GNM003B	81.15	81.9	0.014	GNM007B	58	58.7	0.007
GNM003B	81.9	82.75	0.019	GNM007B	58.7	59.74	0.021
GNM003B	82.75	83.6	0.012	GNM007B	59.74	60.7	0.012
GNM003B	83.6	84.5	0.014	GNM007B	60.7	61.6	0.007
GNM003B	84.5	85.6	0.019	GNM007B	61.6	63.15	0.016
GNM003B	85.6	86.7	0.008	GNM007B	63.15	64.92	0.007
GNM003B	86.7	87.8	0.009	GNM007B	64.92	66.35	0.007
GNM003B	87.8	88.9	0.01	GNM007B	66.35	67.15	0.112
GNM003B	88.9	90	0.01	GNM007B	67.15	68.3	<0.005
GNM004B	1.5	2.1	0.045	GNM007B	68.3	69.43	0.008
GNM004B	2.1	3.6	0.018	GNM007B	69.43	70.35	0.005
GNM004B	3.6	5.15	0.013	GNM007B	70.35	71.8	0.006
GNM004B	5.15	6.7	0.019	GNM007B	71.8	72.65	0.153
GNM004B	6.7	7.7	0.017	GNM007B	72.65	73.52	<0.005
GNM004B	7.7	8.8	0.018	GNM007B	73.52	74.28	0.008
GNM004B	8.8	10	0.012	GNM007B	74.28	75.3	0.156
GNM004B	10	11	0.014	GNM007B	75.3	76.3	0.064
GNM004B	11	12	0.014	GNM007B	76.3	77.2	<0.005
GNM004B	12	13.25	0.017	GNM007B	77.2	78.1	<0.005

Continued

GNM004B	13.25	14.15	0.022		GNM007B	78.1	79.1	0.008	
GNM004B	14.15	15.15	0.071		GNM007B	79.1	80.15	<0.005	
GNM004B	15.15	17	0.02		GNM007B	80.15	81.08	<0.005	
GNM004B	17	18.15	0.016		GNM007B	81.08	81.98	<0.005	
GNM004B	18.15	19.27	0.013		GNM007B	81.98	82.8	0.01	
GNM004B	19.27	21.27	0.018		GNM007B	82.8	84	0.006	
GNM004B	21.27	22.5	0.01		GNM007B	84	85	0.034	
GNM004B	22.5	23.45	0.012		GNM007B	85	86.1	0.025	
GNM004B	23.45	25	0.012		GNM007B	86.1	87.2	0.035	
GNM004B	25	26.15	0.036		GNM007B	87.2	88	0.013	
GNM004B	26.15	28	0.021		GNM007B	88	89	<0.005	
GNM004B	28	29.3	0.012		GNM007B	89	90	0.007	
GNM004B	29.3	30.3	0.014		GNM007B	90	90.94	0.578	2.05m@0.58ppm
GNM004B	30.3	32	0.015		GNM007B	90.94	92.05	0.589	
GNM004B	32	34	0.036		GNM007B	92.05	93.2	0.074	
GNM004B	34	36.1	1.05	2.1m@1.05ppm	GNM007B	93.2	94.4	0.007	
GNM004B	36.1	36.85	0.069		GNM007B	94.4	95.65	<0.005	
GNM004B	36.85	37.65	0.347		GNM007B	95.65	96.6	0.009	
GNM004B	37.65	39.5	0.023		GNM007B	96.6	97.6	<0.005	
GNM004B	39.5	40.5	0.025		GNM007B	97.6	98.8	0.005	
GNM004B	40.5	41.6	0.018		GNM007B	98.8	100	<0.005	

Of the seven points drilled, six intercepted mineralization. The intercepts are summarised by lithology in the table below (Table 2).

Table 2. Gold mineralised area.

Points	Depth	Lithology	Au_ppm
G002B	38.6 m to 40.85 m	Quartz vein	2.25m@0.66ppm
	61.00 m to 64.7 m	Silicified andesite	3.70m@0.99ppm
G003B	17.05 m to 19.50 m	Quartz vein	2.45m@0.97ppm
	60.25 m to 63.95 m	Quartz veinlets in silicified andesite with fine sulphides	3.70m@0.68ppm
G004B	34.00 m to 36.10 m	Contact between Andesite and VS	2.10m@1.05ppm
G005B	31.00 m to 33.45 m	Veins of dark, brecciated quartz with fine sulphides	2.45m@1.64ppm
	36.62 m to 39.00 m	Veins of dark, brecciated quartz with fine sulphides	2.38m@2.89ppm
G006B	48.20 m to 50.25 m	Brecciated quartz veinlets	2.05m@1.49ppm
	69.90 m to 76.15 m	Contact between Andesite and VS	6.25m@0.81ppm
G007B	25.50 m to 27.95 m	Brecciated dark quartz vein with oxidised parts, probably oxidised sulphides	2.45m@1.55ppm
	90.00 m to 92.05 m	Vein of whitish quartz with little mineralisation	2.05m@0.54ppm

Overall, 11 intercepts were identified from the interpretation of the gold assay results. Of these, 8 were controlled by quartz veins, with 7 by smoky quartz veins and 1 by white quartz veins. Mineralization in the Gnimi B zone is controlled by both lithology and structures. In conclusion, structural control takes precedence over lithological control, as contact zones are also interpreted as structures.

The emplacement of the TTGs by the upwelling of plutonic magmatism induced mineralizing fluids, which subsequently used the D2 structures as traps. These fluids originated from the interaction between the volcano-sedimentary host rock and the first-generation granitoids.

5. Discussion

This study, based on the analysis of data from mining holes, aims to decipher the controls on gold mineralization in the Gnimi-Yaboghane B zone. It is part of a broader study of the West African Craton, where gold mineralization is generally associated with greenstone belts and Paleoproterozoic tectono-metamorphic processes. [1] [4] [15] [29] [30]-[33].

The study area consists of volcano-sedimentary rocks, basic rocks, and plutonic rocks metamorphosed during the Eburnian period, as described in other sectors of the West African Craton, notably in the Man Ridge [1] [17] [29] [34]-[35] and in the Kaye and Kédougou-Kéniéba buttonholes [36]. The presence of TTG-trending granitoids, similar to those identified in the Boromo and Houndé belts [2] [4], suggests a comparable tectonic-magmato-metamorphic framework.

Structural analysis of the zone has identified three deformation phases: D1, D2, and D3. This pattern is consistent with observations made in other belts in Burkina Faso, such as Tenkodogo [37] [38], Gaoua, and Manga [16], where up to four deformation phases have been documented (D1 to D4). These deformations played a decisive role in the development and control of gold mineralization. Indeed, several studies indicate that gold mineralization in the West African Craton is mainly controlled by structures developed during phases D2 and D3 [16]-[18] [35] [39] [40].

Structural data and analysis of mineralized intercepts in the study area confirm this trend. Gold is mainly concentrated in smoky quartz veins, formed during the D2 deformation phase. This phase corresponds to the development of NE-SW shear corridors and the establishment of TTGs, which played a major role in the migration and precipitation of mineralizing fluids. In contrast, the weak mineralization observed in the white quartz veins associated with phase D3 suggests that this phase had a more limited impact on gold concentration.

6. Conclusions

This article highlights three groups of geological formations: metavolcano-sedimentary rocks, basic rocks, and the Tonalite-Trondhjemite-Granodiorite (TTG) family. Microscopic analysis of the metavolcano-sedimentary formations shows pressure shadows indicating zones of recrystallization, demonstrating the effects of metamorphism and deformation these formations have undergone. Basic rocks include gabbros with amphibolitic tendencies and metaandesites, forming intercalations with the volcano-sedimentary rocks. The TTG group is represented by granodioritic formations containing angular and rounded enclaves. These formations are hosted within and cross the volcano-sedimentary rocks.

At the end of this study, the structural analysis identified the structures controlling the mineralization: the smoky quartz veins and the white quartz veins. Interpretation of the structures by relative chronology allowed us to distinguish three deformation phases: D1, which trends N-S; D2, which trends NNE-SSW; and D3, which trends E-W.

Overall, the D2 structures are the most mineralized, having been mined by gold panning and intersected by drilling as a favorable zone. These structures can serve as metallotects for further exploration in this area and the South-West region in general. These metallotects should be combined with favorable lithologies and contact zones to produce a favorability map.

Acknowledgements

This work contributes to understanding the control of gold mineralization in the Gnimi-Yaboghane sector, Dano commune, Ioba Province, South-West Region. We thank the person in charge of the semi-mechanised Gnimi project, particularly the Managing Director of the Cooperative Society with a Board of Directors, Burkina Mining, and all his staff for providing accommodation and support for the field analyses. We also thank the head of the Geosciences and Environment Laboratory (LaGE) for preparing the slides and observing them under the microscope, as well as ACLABS Burkina Faso SARL and ALS laboratories for the gold analyses.

Conflicts of Interest

The authors declare no conflicts of interest regarding the publication of this paper.

References

[1] Abouchami, W., Boher, M., Michard, A. and Albarede, F. (1990) A Major 2.1 Ga Event of Mafic Magmatism in West Africa: An Early Stage of Crustal Accretion. *Journal of Geophysical Research*: *Solid Earth*, **95**, 17605-17629. https://doi.org/10.1029/jb095ib11p17605

[2] Lompo, M. (2009) Geodynamic Evolution of the 2.25-2.0 Ga Palaeoproterozoic Magmatic Rocks in the Man-Leo Shield of the West African Craton. A Model of Subsidence of an Oceanic Plateau. *Geological Society*, *London*, *Special Publications*, **323**, 231-254. https://doi.org/10.1144/sp323.11

[3] Vidal, M., Gumiaux, C., Cagnard, F., Pouclet, A., Ouattara, G. and Pichon, M. (2009) Evolution of a Paleoproterozoic "Weak Type" Orogeny in the West African Craton (Ivory Coast). *Tectonophysics*, **477**, 145-159. https://doi.org/10.1016/j.tecto.2009.02.010

[4] Baratoux, L., Metelka, V., Naba, S., Jessell, M.W., Grégoire, M. and Ganne, J. (2011)

Juvenile Paleoproterozoic Crust Evolution during the Eburnean Orogeny (~2.2-2.0 Ga), Western Burkina Faso. *Precambrian Research*, **191**, 18-45. https://doi.org/10.1016/j.precamres.2011.08.010

[5] Chardon, D., Bamba, O. and Traoré, K. (2020) Eburnean Deformation Pattern of Burkina Faso and the Tectonic Significance of Shear Zones in the West African Craton. *BSGF-Earth Sciences Bulletin*, **191**, 2-18. https://doi.org/10.1051/bsgf/2020001

[6] Koffi, A.Y., Thébaud, N., Kouamelan, A.N., Baratoux, L., Bruguier, O., Vanderhaeghe, O., *et al.* (2022) Archean to Paleoproterozoic Crustal Evolution in the Sassandra-Cavally Domain (Côte D'ivoire, West Africa): Insights from Hf and U-Pb Zircon Analyses. *Precambrian Research*, **382**, Article ID: 106875. https://doi.org/10.1016/j.precamres.2022.106875

[7] Sourgou, O. (2024) Caractérisation des leptynites paléoproterozoiques du Centre et du Sud du Burkina Faso (Craton Ouest Africain): Approche petro-géochimique et structurale. Thèse de l'Université Joseph KI-ZERBO, 232 p.

[8] Tagini, B. (1971) Esquisse structurale de la Côte d'Ivoire. Essai de géotectonique régionale. Thèse Univ., 302 p.

[9] Feybesse, J., Billa, M., Guerrot, C., Duguey, E., Lescuyer, J., Milesi, J., *et al.* (2006) The Paleoproterozoic Ghanaian Province: Geodynamic Model and Ore Controls, Including Regional Stress Modeling. *Precambrian Research*, **149**, 149-196. https://doi.org/10.1016/j.precamres.2006.06.003

[10] Grenholm, M., Jessell, M. and Thébaud, N. (2019) A Geodynamic Model for the Paleoproterozoic (Ca. 2.27-1.96 Ga) Birimian Orogen of the Southern West African Craton—Insights into an Evolving Accretionary-Collisional Orogenic System. *Earth-Science Reviews*, **192**, 138-193. https://doi.org/10.1016/j.earscirev.2019.02.006

[11] Vidal, M., Delor, C., Pouclet, A., Simeon, Y. and Alric, G. (1996) Evolution géodynamique de l'Afrique de l'Ouest entre 2.2 Ga et 2 Ga: Le style archéen des ceintures vertes et des ensembles sédimentaires Birimiens du Nord-Est de la Côte d'Ivoire. *Bulletin de la Société Géologique de France*, **167**, 307-319.

[12] Hirdes, W., Davis, D.W., Lüdtke, G. and Konan, G. (1996) Two Generations of Birimian (Paleoproterozoic) Volcanic Belts in Northeastern Côte D'ivoire (West Africa): Consequences for the "Birimian Controversy". *Precambrian Research*, **80**, 173-191. https://doi.org/10.1016/s0301-9268(96)00011-3

[13] Nopeia, M., Imai, A., Yonezu, K., Takahashi, R., Agangi, A. and Jamal, D. (2024) Timing and Origin of Gold Mineralization in the Neoproterozoic Xixano Complex, Mozambique Belt, Northeastern Mozambique: Case Study of the Nanlia and Makorongo Prospects. *Journal of African Earth Sciences*, **218**, Article ID: 105350. https://doi.org/10.1016/j.jafrearsci.2024.105350

[14] Béziat, D., Bourges, F., Debat, P., Lompo, M., Martin, F. and Tollon, F. (2000) A Paleoproterozoic Ultramafic-Mafic Assemblage and Associated Volcanic Rocks of the Boromo Greenstone Belt: Fractionates Originating from Island-Arc Volcanic Activity in the West African Craton. *Precambrian Research*, **101**, 25-47. https://doi.org/10.1016/s0301-9268(99)00085-6

[15] Castaing, C., Billa, M., Milési, J.P., Thiéblemont, D., Le Métour, J., Egal, E. and Donzeau, M. (2003) Notice explicative de la carte géologique et minière du Burkina Faso à 1/1 000 000. Éditions BRGM, 1-147.

[16] Goldfarb, R., Groves, D. and Tomkins, A. (2017) Gold Deposits in Metamorphic Rocks. *Elements*, **13**, 293-299.

[17] Fontaine, A., Eglinger, A., Ada, K., André-Mayer, A., Reisberg, L., Siebenaller, L., *et*

al. (2017) Geology of the World-Class Kiaka Polyphase Gold Deposit, West African Craton, Burkina Faso. *Journal of African Earth Sciences*, **126**, 96-122. https://doi.org/10.1016/j.jafrearsci.2016.11.017

[18] Ouiya, P., Fontaine, A. and Eglinger, A. (2020) Structural and Mineralogical Controls on Gold Mineralization in the Paleoproterozoic of Burkina Faso. *Precambrian Research*, **338**, Article ID: 105605.

[19] Hottin, J. and Ouédraogo, O.F. (1975) Notice explicative de la carte géologique à 1/1000000 de la république de Haute Volta. Archives D.G.M., 58 p.

[20] Feybesse, J. and Milési, J. (1994) The Archaean/Proterozoic Contact Zone in West Africa: A Mountain Belt of Décollement Thrusting and Folding on a Continental Margin Related to 2.1 Ga Convergence of Archaean Cratons? *Precambrian Research*, **69**, 199-227. https://doi.org/10.1016/0301-9268(94)90087-6

[21] BRGM/BUVOGMI (1983) Syndicat de Recherches de la Volta Noire. Permis de Recherche de la Volta Noire. Prospection or 1983. 83 RDM 057 AF.

[22] Le Metour, J., Chevremont, P., Donzeau, M., *et al.* (2003) Notice explicative de la Carte géologique du Burkina Faso à 1/200 000; Feuille Houndé.

[23] Kote, S., *et al.* (2003) Notice explicative de la Carte géologique du Burkina Faso à 1/200 000; Feuille Léo.

[24] Naba, S., Lompo, M., Debat, P., Bouchez, J.L. and Béziat, D. (2004) Structure and Emplacement Model for Late-Orogenic Paleoproterozoic Granitoids: The Tenkodogo-Yamba Elongate Pluton (Eastern Burkina Faso). *Journal of African Earth Sciences*, **38**, 41-57. https://doi.org/10.1016/j.jafrearsci.2003.09.004

[25] Yaméogo, A.O., Naba, S. and Traor, S.A. (2020) Caractères pétrographiques et géochimiques des granitoïdes de la région de Dori au nord-est du Burkina Faso. Craton Ouest Africain. *Afrique Science*, **16**, 375-395.

[26] Boher, M., Abouchami, W., Michard, A., Albarede, F. and Arndt, N.T. (1992) Crustal Growth in West Africa at 2.1 Ga. *Journal of Geophysical Research*: *Solid Earth*, **97**, 345-369. https://doi.org/10.1029/91jb01640

[27] Soumaïla, A. and Garba, Z. (2006) Le métamorphisme des formations de la ceinture de roches vertes birimienne (Paléoprotérozoïque) de Diagorou-Darbani (Liptako. Niger. Afrique de l'Ouest). *African Geosciences Review*, **13**, 107-128.

[28] Vegas, N., Naba, S., Bouchez, J.L. and Jessell, M. (2007) Structure and Emplacement of Granite Plutons in the Paleoproterozoic Crust of Eastern Burkina Faso: Rheological Implications. *International Journal of Earth Sciences*, **97**, 1165-1180. https://doi.org/10.1007/s00531-007-0205-z

[29] Caby, R., Delor, C. and Agoh, O. (2000) Lithologie, structure et métamorphisme des formations birimiennes dans la région d'Odienné (Côte d'Ivoire): Rôle majeur du diapirisme des plutons et des décrochements en bordure du craton de Man. *Journal of African Earth Sciences*, **30**, 351-374. https://doi.org/10.1016/s0899-5362(00)00024-5

[30] Ducellier, H. (1963) Géologie de l'Afrique de l'Ouest. BRGM, 88, 403 p.

[31] Hein, K.A.A. (2016) The Bagassi Gold Deposits on the Eastern Margin of the Houndé Greenstone Belt, Burkina Faso. *Ore Geology Reviews*, **78**, 660-666. https://doi.org/10.1016/j.oregeorev.2015.10.028

[32] Pons, J., Barbey, P., Dupuis, D. and Léger, J.M. (1995) Mechanisms of Pluton Emplacement and Structural Evolution of a 2.1 Ga Juvenile Continental Crust: The Birimian of Southwestern Niger. *Precambrian Research*, **70**, 281-301. https://doi.org/10.1016/0301-9268(94)00048-v

[33] Koffi, Y.H., Zongo, W.P.P., Mathieu, N. and Wenmenga, U. (2024) Gold Mineralisation in the Intiédougou Prospect (Diébougou District) in Southwest Burkina Faso, West African Craton. *Journal of Minerals and Materials Characterization and Engineering*, **12**, 63-77. https://doi.org/10.4236/jmmce.2024.121005

[34] Zongo, W.P.P., Wenmenga, U. and Koffi, Y.H. (2017) Caractérisation minéralogique et pétrochimique des serpentinites de Tambogo: Ceinture des roches vertes birimiennes de Kaya-Goren. Burkina Faso. *Bulletin de l'Institut Scientifique*, *Rabat*. *Section Sciences de la Terre*, **38**, 81-94.

[35] Dioh, E., Béziat, D., Debat, P., Grégoire, M. and Ngom, P.M. (2006) Diversity of the Palaeoproterozoic Granitoids of the Kédougou Inlier (Eastern Sénégal): Petrographical and Geochemical Constraints. *Journal of African Earth Sciences*, **44**, 351-371. https://doi.org/10.1016/j.jafrearsci.2005.11.024

[36] Trinquard, R., *et al*. (2003) Notice explicative de la carte géologique du Burkina Faso à l'échelle 1/200000; Feuille Tenkodogo. BRGM, 53 p.

[37] Tshibubudze, A., Hein, K.A.A. and McCuaig, T.C. (2015) The Relative and Absolute Chronology of Strato-Tectonic Events in the Gorom-Gorom Granitoid Terrane and Oudalan-Gorouol Belt, Northeast Burkina Faso. *Journal of African Earth Sciences*, **112**, 382-418. https://doi.org/10.1016/j.jafrearsci.2015.04.008

[38] Groves, D.I., Goldfarb, R.J., Gebre-Mariam, M., Hagemann, S.G. and Robert, F. (1998) Orogenic Gold Deposits: A Proposed Classification in the Context of Their Crustal Distribution and Relationship to Other Gold Deposit Types. *Ore Geology Reviews*, **13**, 7-27. https://doi.org/10.1016/s0169-1368(97)00012-7

[39] Tomkins, A.G. (2013) A Biogeochemical Influence on the Secular Distribution of Orogenic Gold. *Economic Geology*, **108**, 193-197. https://doi.org/10.2113/econgeo.108.2.193

[40] Eglinger, A., Thébaud, N., Zeh, A., Davis, J., Miller, J., Parra-Avila, L.A., *et al*. (2017) New Insights into the Crustal Growth of the Paleoproterozoic Margin of the Archean Kéména-Man Domain, West African Craton (Guinea): Implications for Gold Mineral System. *Precambrian Research*, **292**, 258-289. https://doi.org/10.1016/j.precamres.2016.11.012